Applied Mathematical Modelling 39 (2015) 4767–4780

Contents lists available at ScienceDirect

Applied Mathematical Modelling

journal homepage: www.elsevier.com/locate/apm

Modeling the arterial wall mechanics using a novel high-order viscoelastic fractional element

J.M. Pérez Zerpa [a,*], A. Canelas [a], B. Sensale [a], D. Bia Santana [b], R.L. Armentano [c]

[a] Instituto de Estructuras y Transporte, Facultad de Ingeniería, Universidad de la República, PC 11300 Montevideo, Uruguay
[b] Departamento de Fisiología, CUiiDARTE, Facultad de Medicina, Universidad de la República, PC 11800 Montevideo, Uruguay
[c] Grupo de Ingeniería Aplicada a los Procesos Biológicos y Agrícolas, Centro Universitario Regional Noroeste, Universidad de la República, Paysandú, Uruguay

ARTICLE INFO

Article history:
Received 23 May 2014
Received in revised form 9 March 2015
Accepted 1 April 2015
Available online 24 April 2015

Keywords:
Inverse problems
Viscoelasticity
Fractional viscoelasticity models
Arterial wall mechanics

ABSTRACT

The fractional viscoelastic models (FVMs) have provided promising results for modeling the behavior of complex materials such as polymers and living tissues. These viscoelastic models are composed by springs, dashpots and the fractional element called spring-pot. In this paper we prove that the accuracy of these models can be improved through the use of a modified version of the spring-pot element, called high-order spring-pot (HOSP).

We describe and implement a numerical method for characterization of mechanical properties of FVMs. The method consists of minimizing the misfit among experimental measures of strains or stresses and the respective values predicted by the model. The method is validated by solving four numerical examples. In the first three examples the data is artificially generated using different models such as the Double Maxwell-arm Wiechert one. The characterization is performed using FVMs models including the traditional spring-pot element and the new HOSP element proposed in this article. In these examples we assume small strains and homogeneous material properties. In a final example the method is applied to the characterization of the mechanical properties of FVMs using stress–strain data obtained from *in vitro* ovine arterial wall measurements reported in the literature.

The results obtained show that the proposed method properly determines the mechanical parameters even in presence of noise in the data. In addition, it is evident from the results that the proposed modification of the spring-pot element increases the accuracy of the FVMs models. The results obtained allow us to conclude that the FVMs can model better the behavior of complex materials when a HOSP element is included. In particular, it was shown that these models are appropriate for modeling the arterial wall mechanics with higher accuracy, as well as other materials with complex behavior.

1. Introduction

The behavior of viscoelastic materials is usually represented by simple models composed by elastic and viscous elements, which may be linear springs and dashpots, respectively. These rheological models have been widely used for modeling the behavior of several materials, such as concrete [1]. In [2,3] it is pointed out that living tissues behavior should be generally considered viscoelastic, and we can find in the literature applications of these models to the modeling of a broad set of living tissues [4–6]. There exists a particular interest in the modeling of the arterial wall behavior, motivated by the relevance of

* Corresponding author.

http://dx.doi.org/10.1016/j.apm.2015.04.018
0307-904X/

the Atherosclerotic Cardiovascular Disease (ACD) in the human death toll [7]. Viscoelastic models have been widely applied to the arterial wall mechanics modeling [8,9]. However, Lakes [10] pointed out that simple models composed by a small number of springs and dashpots must be used only with a pedagogic purpose, since real materials are not usually describable by these models. This statement have been confirmed by Wang et al. [6] who have shown that by increasing the number of elements ones improves the accuracy of the rheological models applied to the modeling of living tissues.

We note also that there are many papers in the literature dealing with the development of complex nonlinear elastic models for arterial wall modeling. In particular, the arterial wall tissue is anisotropic, and has been modeled considering histological information such as the fiber orientation in each layer [11]. Recently, nonlinear effects have also been considered in viscoelastic models [12]. In this article we do not consider neither geometric nor material nonlinearities.

Fractional viscoelastic models (FVMs) are those that include at least one fractional element, also known as spring-pot. The spring-pot element represents an intermediate behavior between a linear spring and a linear dashpot. This intermediate behavior is mathematically represented by defining the stress proportional to the fractional derivative of the strain, i.e. $\sigma \propto D^{\alpha}\varepsilon$, where the derivative order α is considered another mechanical parameter, called fractional parameter. To the authors knowledge, in all applications of FVMs considered in the literature, the fractional parameter is a real number within the interval $[0, 1]$.

The first applications of fractional models were reported in the early twentieth century [13]. Throughout the years the interest in the matter have been increasing and important aspects were improved such as new mathematical definitions of the fractional derivative with appropriate physical interpretations [14,15]. In the 80's, Bagley and Torvik [16] presented links between molecular theories and macroscopic fractional viscoelastic models. Since then, they and other authors [17,18] have contributed to the determination of algebraic constraints for the material parameters of the models taking into account thermodynamics constraints.

FVMs are recognized to be well suited for modeling the behavior of real complex materials such as anisotropic structural elements [19], polymers [20,21] and chemical compounds [14]. For living tissues, the FVMs have been successfully applied to the characterization of cells mechanical properties [22], as well as the modeling of the arterial wall mechanics [23–25].

The use of several springs and dashpots in certain arrangements provides constitutive equations with integer derivative orders higher than one. Recently, it was shown that the use of these models produces accurate results [26]. In this paper we use a fractional element that we call high-order spring-pot (HOSP), which is defined by setting the upper bound of the fractional parameter equal to 2. We use FVMs with one HOSP and prove its ability to reproduce the behavior of complex models with higher accuracy. In Appendix B, it is presented a thermodynamic justification of this new upper bound.

In Section 3 we describe a method for characterization of mechanical parameters of FVMs, including the fractional parameter. The numerical method obtains the parameters by solving a nonlinear optimization problem, using a fitness function that depends on the coefficients of the discrete Fourier transform of the given data.

In Section 4 a validation of the proposed method that is performed by studying some examples with numerically generated and experimental data is presented. The experimental data used in this paper is part of the data presented in [9], and consists of measurements of pressure and diameter of arterial wall segments of healthy sheeps. The results obtained show that the HOSP provides higher accuracy in the modeling of the behavior of complex materials when compared against the traditional spring-pot.

Preliminary results of this work were presented in [27]. A more detailed description of the characterization method is presented here, and the theoretical justification about the use of the HOSP element is published in this paper for the first time. Some new insightful examples are presented, as well as a deeper discussion of the results and the advantages of the HOSP element over the traditional spring-pot for the modeling of living tissues.

2. Preliminaries

In this section we present the basic concepts of fractional calculus, some important properties of the Fourier transform and the three viscoelastic models used through the article.

2.1. Fractional calculus

The fractional calculus theory introduces and studies several possible generalizations of the concept of derivative of a function of real number or even complex number order. During the twentieth century it has been used as an appropriate approach for modeling the behavior of viscoelastic materials [16]. In this field, the derivatives of a real number order, also called fractional derivatives, are used to define structural elements for which the stress response is intermediate between that of a spring and that of a dashpot, i.e. the responses corresponding to a zero or a first order derivative of the strain, respectively.

There are different possible definitions for the fractional derivatives of a function, in this paper we will consider the Riemann–Liouville definition with lower terminal as $-\infty$, given by the following expression:

$$D^{\alpha}f(t) = \frac{1}{\Gamma(n-\alpha)} \int_{-\infty}^{t} \frac{f^{(n)}(\tau)}{(t-\tau)^{\alpha+1-n}}\, d\tau \quad n-1 < \alpha < n. \tag{1}$$

This derivative is recognized as a proper definition for steady-state processes such as in modeling the response of viscoelastic materials submitted to a given periodic load [15, p. 80]. This definition satisfies properties such as linearity and composition of derivatives, and the following useful property:

$$D^{\alpha}e^{i\omega t} = (i\omega)^{\alpha}e^{i\omega t} \quad \forall t \in \mathbb{R} \quad \forall \alpha \in \mathbb{R}. \tag{2}$$

In the expression above, the value $i^{\alpha} = \cos\left(\alpha\frac{\pi}{2}\right) + i\sin\left(\alpha\frac{\pi}{2}\right)$, which is also the value computed by the numerical implementations using the software GNU-Octave [28].

2.2. Applying the DFT

Given $y(t)$, a periodic continuous function for the magnitude y, let us consider that an acquisition is performed in N times starting at $t = 0$. The discrete signal is given by

$$y_n = y(T \cdot n) \quad n = 0, \ldots, N-1, \tag{3}$$

where T is the time between samples. If $f_s = 1/T$ is the sampling frequency (the number of samples per time unit) then, we can write $y_n = y\left(\frac{n}{f_s}\right)$. Let us define the Discrete Fourier Transform DFT: $\mathbb{C}^N \to \mathbb{C}^N$, as a vectorial function $\mathbf{Y} = \mathrm{DFT}(\mathbf{y})$, where the k-th entry of $\mathbf{Y}$ is given by

$$Y_k = \sum_{n=0}^{N-1} y_n \cdot e^{-i\omega_k \frac{n}{f_s}} \quad k = 0, \ldots, N-1, \tag{4}$$

where $\omega_k = 2\pi k\frac{f_s}{N}$ is the k-th frequency. The Inverse DFT is the inverse function of the DFT transform, i.e. $\mathbf{y} = \mathrm{IDFT}(\mathbf{Y})$, and the n-th entry of $\mathbf{y}$ is given by

$$y_n = \frac{1}{N}\sum_{k=0}^{N-1} Y_k \cdot e^{i\omega_k \frac{n}{f_s}} \quad n = 0, \ldots, N-1. \tag{5}$$

Let us assume that the continuous function $y(t)$ can be decomposed as a sum of exponential functions

$$y(t) = \frac{1}{N}\sum_{k=0}^{N-1} Y_k\, e^{i\omega_k t} \quad \omega_k = 2\pi f_s \frac{k}{N}. \tag{6}$$

If we consider the times $t = n/f_s$, then the values Y_k can be obtained by using the DFT. Using the property given by Eq. 2 we obtain

$$D^{\alpha}y(t) = \frac{1}{N}\sum_{k=0}^{N-1} (i\omega_k)^{\alpha} Y_k\, e^{i\omega_k t}. \tag{7}$$

Once again, considering the times $t = n/f_s$, we obtain the expression of the DFT of a fractional derivative for the k-th frequency as:

$$\left(\mathrm{DFT}(D^{\alpha}y(t))\right)_k = (i\omega_k)^{\alpha} Y_k. \tag{8}$$

In a similar way, we can see that a constant signal $y(t) = c$ has the k-th component of the DFT given by

$$(\mathrm{DFT}(c))_k = cN\delta_{k0}, \tag{9}$$

where δ_{ij} is the Kronecker delta.

2.3. Viscoelastic models

In this section we describe two well-known viscoelastic models and a fractional variation of one of them. These models are described in [29].

Standard Linear Solid. In the Standard Linear Solid (SLS) the material model consists of an arrangement of two springs and one dashpot, as can be seen in Fig. 1(a). The positive material parameters E_0 and E_1 correspond to the stiffness of the springs and the positive value η_1 is the viscosity of the dashpot. This model provides the following constitutive equation:

$$\sigma + \frac{\eta_1}{E_1}\dot{\sigma} = E_0(\varepsilon - \varepsilon_0) + \frac{(E_1 + E_0)}{E_1}\eta_1\,\dot{\varepsilon}, \tag{10}$$

where σ is the stress in the material, ε is the strain, and ε_0 is the strain corresponding to a static stress-free configuration. By defining the following two positive material parameters:

$$\tau_{\sigma} = \frac{\eta_1}{E_1}, \quad \tau_{\varepsilon} = \frac{E_1 + E_0}{E_1 E_0}\eta_1, \tag{11}$$

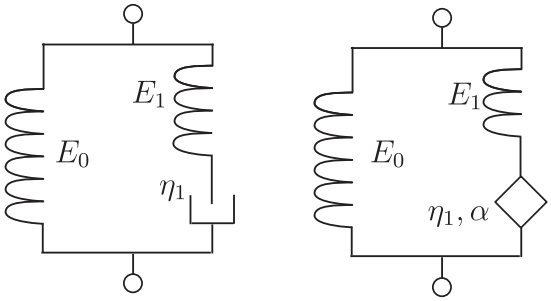

Fig. 1. Left – Standard Linear Solid model. Right – Fractional Standard Linear Solid model.

where τ_σ and τ_ε are called *relaxation time* and *creep time*, respectively, which have dimension of time, the constitutive equation can be rewritten as:

$$\sigma + \tau_\sigma \dot{\sigma} = E_0((\varepsilon - \varepsilon_0) + \tau_\varepsilon \dot{\varepsilon}). \tag{12}$$

Fractional Standard Linear Solid. In a fractional element, called spring-pot, the stress is proportional to the fractional derivative of the deformation:

$$\sigma = E_1 \tau_\sigma^\alpha D^\alpha \varepsilon, \tag{13}$$

where α is the fractional parameter. In the literature this parameter is considered a real number in the domain $[0, 1]$. However, in Appendix B we show that it is thermodynamically admissible to allow α to be in the domain $[0, 2]$. This modified spring-pot is what we call the high-order spring-pot (HOSP).

If we replace the dashpot by a spring-pot in the SLS model, see Fig. 1(b), we obtain the Fractional Standard Linear Solid (FSLS), which has the following constitutive equation:

$$\sigma + \tau_\sigma^\alpha D^\alpha \sigma = E_0 \left((\varepsilon - \varepsilon_0) + \frac{(E_1 + E_0)}{E_0} \tau_\sigma^\alpha D^\alpha \varepsilon \right). \tag{14}$$

In a more compact form the constitutive equation can be written as

$$\sigma + \tau'_\sigma D^\alpha \sigma = E_0 \left((\varepsilon - \varepsilon_0) + \tau'_\varepsilon D^\alpha \varepsilon \right), \tag{15}$$

where

$$\tau'_\sigma = \left(\frac{\eta_1}{E_1} \right)^\alpha, \quad \tau'_\varepsilon = \frac{E_1 + E_0}{E_0} \tau'_\sigma. \tag{16}$$

It is important to note that the parameters τ'_σ and τ'_ε have dimension of [time$^\alpha$]. It is easy to see that this model represents the SLS model when $\alpha = 1$ is considered.

Double Maxwell-arm Wiechert. The Double Maxwell-arm Wiechert (DMW) model corresponds to an arrangement of three springs and two dashpots, see Fig. 2. The constitutive equation is given by:

$$\sigma + \chi_1 \dot{\sigma} + \chi_2 \ddot{\sigma} = E_0((\varepsilon - \varepsilon_0) + \nu_1 \dot{\varepsilon} + \nu_2 \ddot{\varepsilon}), \tag{17}$$

where

$$\chi_1 = \tau_{\sigma 1} + \tau_{\sigma 2}, \quad \chi_2 = \tau_{\sigma 1} \tau_{\sigma 2}, \tag{18}$$

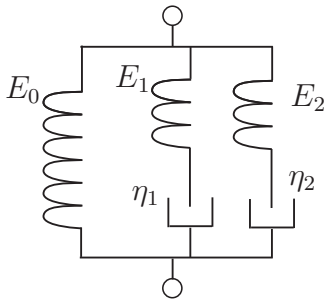

Fig. 2. Viscoelastic Double Maxwell-arm Wiechert model.

$$\nu_1 = \tau_{\sigma 1} + \tau_{\sigma 2} + \upsilon_1 + \upsilon_2, \quad \nu_2 = \tau_{\sigma 1}\tau_{\sigma 2} + \upsilon_1\tau_{\sigma 2} + \upsilon_2\tau_{\sigma 1} \tag{19}$$

and

$$\tau_{\sigma 1} = \frac{\eta_1}{E_1}, \quad \tau_{\sigma 2} = \frac{\eta_2}{E_2}, \quad \upsilon_1 = \frac{\eta_1}{E_0}, \quad \upsilon_2 = \frac{\eta_2}{E_0}. \tag{20}$$

In [6] this model is presented as one of the complex viscoelastic models with the capability of fitting experimental biologic data with higher accuracy than the SLS model.

3. Characterization method

Let us consider the FSLS constitutive model given by five material parameters, which can be separated in one fractional parameter α and other four mechanical parameters represented by the vector $\mathbf{x}$. Using this notation the constitutive equation is,

$$\sigma + x_4 D^\alpha \sigma = -x_1 + x_2\varepsilon + x_3 D^\alpha \varepsilon, \tag{21}$$

where x_1 is positive for a positive strain ε_0. Let us consider that stresses and strains are acquired in N times. Applying the DFT to both terms and using the properties given by Eqs. (8) and (9) we obtain the following identity:

$$\sum_{n=0}^{N-1}\left((1 + x_4(i\omega_n)^\alpha)Q_n + x_1 N\delta_{n0} - \left(x_2 + x_3(i\omega_n)^\alpha\right)U_n\right)e^{i\omega_n t} = 0, \tag{22}$$

where $\mathbf{Q}$ and $\mathbf{U}$ represent the DFT vectors of the signals acquired for σ and ε, respectively, and ω_n is the above-mentioned n-frequency. Since this identity is valid for all times and any stress and strain signals, we obtain the following system of equations

$$(\mathbf{I} + x_4\mathbf{\Lambda}_\alpha)\mathbf{Q} + x_1\mathbf{D} - (x_2\mathbf{I} + x_3\mathbf{\Lambda}_\alpha)\mathbf{U} = 0, \tag{23}$$

where $\mathbf{\Lambda}_\alpha$ is a diagonal matrix with coefficients $(\mathbf{\Lambda}_\alpha)_{nn} = (i\omega_{n-1})^\alpha$, and $\mathbf{D}$ is a vector with $D_i = \delta_{i1}N$. Let us consider that the strains and stresses are measured and represented by the signals $\tilde{\varepsilon}$ and $\tilde{\sigma}$ respectively, and their respective DFT coefficient vectors represented by $\tilde{\mathbf{U}}$ and $\tilde{\mathbf{Q}}$. We denote by ε and σ the strains and stresses solution to (21), i.e. the signals given by the model for certain mechanical parameters $(\mathbf{x}, \alpha)$.

In a similar way as it is done in [9], we assume that either the stress or the strain given by the model is equal to the measured signal. For the numerical results presented in this paper we assume that the measured stress, and therefore its DFT vector, has no error, thus $\tilde{\mathbf{Q}} = \mathbf{Q}$. We can obtain the strain DFT vector given by the model from Eq. (23):

$$U_n(\mathbf{x}, \alpha) = \frac{(1 + x_4(i\omega_n)^\alpha)\tilde{Q}_n + x_1 N\delta_{n0}}{x_2 + x_3(i\omega_n)^\alpha}, \quad n = 0, \ldots, N-1. \tag{24}$$

Then, the problem of characterization is to determine the best parameters to fit the experimental strain with the one given by the model. This characterization problem can be written as

$$\begin{cases} \min\limits_{\mathbf{x},\alpha} f(\mathbf{x}, \alpha) \\ \text{subject to} \\ \quad x_i \geqslant 0 \quad i = 2, \ldots, 4 \\ \quad \mathbf{x} \in \mathbb{R}^4 \quad \alpha \in I_\alpha \end{cases} \quad \text{where} \quad f(\mathbf{x}, \alpha) = \frac{\|\mathbf{U}(\mathbf{x}, \alpha) - \tilde{\mathbf{U}}\|^2}{\|\tilde{\mathbf{U}}\|^2}, \tag{25}$$

where f is the fitness, given by the relative error of the DFT coefficients of the strain of the model, and I_α is a given real interval. Note that there is no constraint in the sign of x_1, i.e. the optimal stress-free strain can be negative or positive. This inverse problem is solved using an iterative numerical method which is described below.

Since the fractional parameter varies in a real interval, problem (25) is solved for all fractional parameters in a given discrete set of values $S_\alpha = \{\alpha_s + i\Delta\alpha \,|\, i = 1, \ldots, N_\alpha\}$. The optimization problem is solved for each value α in the set. In order to improve the speed of the process, it is convenient to provide an appropriate initial point. If we replace in (23) $\mathbf{Q}$ and $\mathbf{U}$ by $\tilde{\mathbf{Q}}$ and $\tilde{\mathbf{U}}$, respectively, we obtain:

$$(\mathbf{I} + x_4\mathbf{\Lambda}_\alpha)\tilde{\mathbf{Q}} + x_1\mathbf{D} - (x_2\mathbf{I} + x_3\mathbf{\Lambda}_\alpha)\tilde{\mathbf{U}} = 0. \tag{26}$$

This equation can be used to obtain a reasonable initial point by solving the linear least squares problem $\min_{\mathbf{x}\in\mathbb{R}^4}\|\mathbf{A}\mathbf{x} - \mathbf{b}\|^2$ where

$$\mathbf{A} = [\mathbf{D} \;\; -\tilde{\mathbf{U}} \;\; -\Lambda_\alpha\tilde{\mathbf{U}} \;\; \Lambda_\alpha\tilde{\mathbf{Q}}], \quad \mathbf{b} = \tilde{\mathbf{Q}}. \tag{27}$$

The parameters x_2, x_3 and x_4 are nonnegative, so that a nonnegative linear squares solver must be used to solve the problem, such as the GNU Octave function `lsqnonneg`. The use of this initial point has shown a considerable improvement in the performance of the optimization algorithm for problem (25).

After solving problem (25) for each value $\alpha \in S_\alpha$ we define the optimal fractional parameter $\alpha = \alpha^*$ as the one with the lower fitness $f(x^*, \alpha^*)$ where $\mathbf{x}^*$ denotes the solution of (25) for α^*:

$$\mathbf{x}^* = \arg\min_{\mathbf{x}}(f(\mathbf{x}, \alpha^*)), \quad \text{where} \quad \alpha^* = \arg\min_{\alpha}(\arg\min_{\mathbf{x}}(f(\mathbf{x}, \alpha))). \tag{28}$$

Frequencies of the DFT. Although the DFT provides a vector of coefficients with as many entries as signal measurements, a lower number of coefficients must be used. Considering the criterion applied in [23] we choose from the vector of coefficients the entries associated with the fifteen first harmonics of the fundamental frequency of the signal. This reduced DFT vector is actually used to evaluate the fitness of problem (25), in the characterization method implemented. The fundamental frequency is estimated through an analysis of the power spectrum of the signal and its accuracy is given by the sampling frequency f_s and the length of the acquired data N.

4. Results

In this section we present results obtained using the proposed characterization method for three examples with artificially generated data and one with experimental data. The solution to (25) is obtained by using the `sqp` solver from the `optim` package of the GNU Octave software [28] and the initial point is obtained using the Octave function `lsqnonneg`. For each example the characterization method is applied using the FSLS model considering the traditional spring-pot and the HOSP element.

Artificial data. In Examples 1 and 2 artificial $\tilde{\sigma}$ and $\tilde{\varepsilon}$ signals are generated using known mechanical and fractional parameters. In Example 3 pressure and diameter artificial data are generated considering a thin-walled vessel with variable internal pressure including the inertial terms in the governing equations of the problem.

Experimental data. In Example 4, stress and strain data are obtained from pressure and diameter experimental data.

Error measure. A relative error is defined using the L-2 norm in order to measure the misfit after characterization. The error measures the misfit between the strain given by the model ε and the solution strain $\tilde{\varepsilon}$. The expression of the error is given by

$$Error = \frac{\|\varepsilon - \tilde{\varepsilon}\|_{L_2}}{\|\tilde{\varepsilon}\|_{L_2}} = \frac{\sqrt{\int_0^T |\varepsilon(t) - \tilde{\varepsilon}(t)|^2 \, dt}}{\sqrt{\int_0^T |\tilde{\varepsilon}(t)|^2 \, dt}}. \tag{29}$$

All numerical results where obtained using an Intel i7 processor running GNU Octave version 3.8.0. The execution times where for all cases lower than a few minutes.

4.1. Example 1 – Artificial FSLS data

In this example the characterization method is applied to artificially generated data. The stress–strain data is generated using the FSLS model with known mechanical parameters, and noise is added in order to obtain results about the stability of the method. The goal of this example is to verify that the implementation of the characterization method effectively obtains the mechanical parameters used to generate the data even in the presence of some level of noise.

Strain values are generated by using the following formula

$$\tilde{\varepsilon}(t) = \varepsilon_{0c} + \sum_{k=1}^{2} \varepsilon_{kc} \cos(\lambda_k t) + \varepsilon_{ks} \sin(\lambda_k t), \tag{30}$$

where the frequencies are $\lambda_k = 2\pi \times 1.8 \times k$, and the amplitudes are $\varepsilon_{0c} = 0.15, \varepsilon_{1c} = 0.075, \varepsilon_{1s} = 0.025, \varepsilon_{2c} = 0.3\varepsilon_{1c}$, and $\varepsilon_{2s} = 0.3\varepsilon_{1s}$. The values of $\tilde{\sigma}$ are calculated using the FSLS model with the mechanical parameters $E = 1$ kPa, $\tau_\varepsilon = 0.1\text{s}^\alpha$, $\tau_\sigma = 0.01\text{s}^\alpha$, and $\alpha = 0.64$. We assume a stress-free strain $\varepsilon_0 = 0$. The data with noise $\hat{\varepsilon}$ and $\hat{\sigma}$ are obtained in the same manner as in [21] through the following expressions:

$$\hat{\varepsilon}(t) = \tilde{\varepsilon}(t) + v(t)\xi\sqrt{var(\tilde{\varepsilon})}, \quad \hat{\sigma}(t) = \tilde{\sigma}(t) + w(t)\xi\sqrt{var(\tilde{\sigma})}, \tag{31}$$

where v and w are randomly generated, corresponding to a standard distribution of zero mean and unit deviation, and ξ is the noise level. The first data set has zero noise level, while the data sets 2 and 3 have noise level 1% and 2%, respectively.

The discrete set S_α is defined in the interval $I_\alpha = [0.2, 1]$ with a step 0.005. Note that for $\alpha = 0$, the material model is purely elastic, and its actual stiffness is given by three redundant parameters which cannot be determined univocally. Small values of α will then render ill-conditioned problems, that is why a positive lower bound is used in the interval I_α.

Fig. 3 shows the optimum fitness obtained for each value of α for the three data sets. The numerical results are presented in Table 1. The error of the fractional parameter in the data without noise is given by the step used in the definition of S_α, in this case it is 0.005 which represents a precision below 0.4%. It is important to remark also that the strain ε_0 obtained by the method is negligible when compared against the largest strain values of the signal.

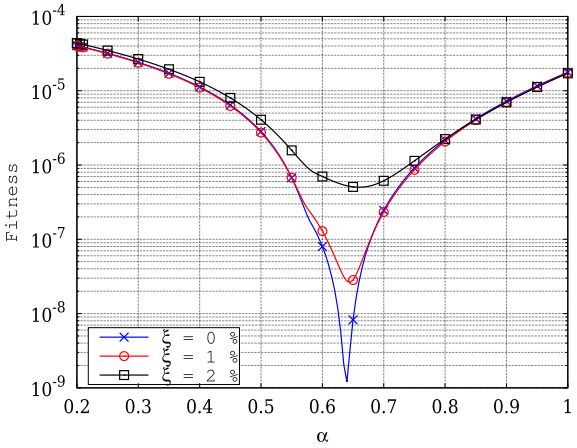

Fig. 3. Example 1 optimum fitness results.

Table 1
Results of Example 1.

Parameter	Solution	$\xi = 0\%$	$\xi = 1\%$	$\xi = 2\%$
$\varepsilon_0\,(10^{-4})$	0	0.1613	$[-20.71, 7.67]$	$[-17.83, 1.6]$
$E\,(\text{kPa})$	1	1.00003	$[0.986, 1.00493]$	$[0.988, 1.0008]$
$\tau'_\varepsilon\,(\text{s}^\alpha)$	0.1	0.0998	$[0.0985, 0.1047]$	$[0.0992, 0.1049]$
$\tau'_\sigma\,(\text{s}^\alpha)$	0.01	0.00989	$[0.0067, 0.0114]$	$[0.005, 0.013]$
α	0.64	0.64	$[0.615, 0.65]$	$[0.62, 0.65]$
Fitness (10^{-9})		1.208	$[65.28, 149.5]$	$[208.69, 433.51]$
Error (10^{-4})		2.8038	$[37.87, 38.91]$	$[74.79, 76.07]$

Since the noise introduced in the data sets 2 and 3 is randomly generated, their corresponding results are expressed in Table 1 in terms of the range of values obtained in five runs. For all parameters, except for τ_σ, the relative error in the parameter is of the order of the noise level introduced in the data.

Fig. 4 depicts the hysteresis loops given by the model using the optimal mechanical parameters (crosses) and the hysteresis loops of the solution data (circles) for the data sets 1 and 3.

The results obtained let us conclude that the method is appropriate for the characterization of mechanical and fractional parameters of a FSLS constitutive model. Noise was added to the data and the results show that the method is able to characterize the mechanical parameters with an error of the order of the noise level introduced, except for the τ_σ parameter. The method is then stable and able for its use with experimental data. Respect to the results for the parameter τ_σ, we can appreciate sensitivity respect to the noise, being this fact already reported in the literature [9]. However, we are specially interested in the ability of the method to determine the fractional parameter, which, as we will show below, is the crucial one in complex behavior modeling.

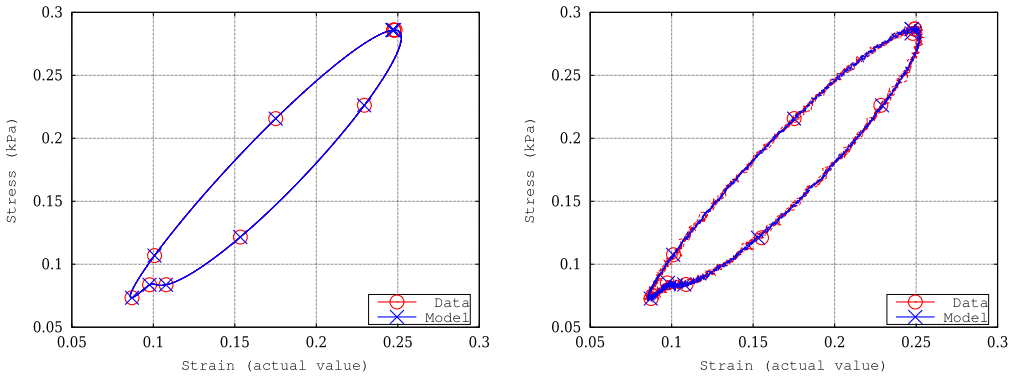

Fig. 4. Example 1: Left – hysteresis obtained for $\xi = 0$. Right – hysteresis obtained for $\xi = 2\%$.

4.2. Example 2 – Artificial DMW data

In this example the method is applied to stress and strain data artificially generated using a DMW model, and characterization is performed using the presented FSLS model. The aim of this example is to test the ability of the FSLS model to represent the behavior of viscoelastic models composed by several springs and dashpots.

As a first approach to the modeling of living tissues, in this example the values of the mechanical parameters considered are the average values obtained in recent literature for modeling porcine tissue behavior with a DMW model [6]. The first data set will be generated using the mechanical parameters obtained for porcine spleen $E_0 = 1.22$ kPa, $E_1 = 1.03$ kPa, $\eta_1 = 2.44$ kPa s, $E_2 = 0.66$ kPa and $\eta_2 = 38.22$ kPa s, and the second data set is obtained using the porcine liver mechanical parameters $E_0 = 3.53$ kPa, $E_1 = 7.74$ kPa, $\eta_1 = 21.81$ kPa s, $E_2 = 5.62$ kPa and $\eta_2 = 410.81$ kPa s. In both cases a stress-free strain $\varepsilon_0 = 0$ is considered.

Although the data sets are generated using the same procedure as in Example 1, in this case the amplitudes are $\varepsilon_{0c} = 0.15 \times 10^{-3}, \varepsilon_{1c} = 0.075 \times 10^{-3}, \varepsilon_{1s} = 0.025 \times 10^{-3}, \varepsilon_{2c} = 0.3\varepsilon_{1c}, \varepsilon_{2s} = 0.3\varepsilon_{1s}, \varepsilon_{3c} = 0.1\varepsilon_{1c}$ and $\varepsilon_{3s} = 0.1\varepsilon_{1s}$. The frequencies are also given by $\lambda_k = 2\pi \times 1.8 \times 10^{-3} \times k$ with $k = 1, 2, 3$. These values are chosen with the purpose of obtaining stresses in the order of magnitude of those obtained in [6]. In this example the data sets are not polluted with noise.

In order to compare the results obtained for the FSLS model using the traditional spring-pot and the HOSP element, we perform a characterization considering the traditional spring-pot and the HOSP. The results obtained are presented in Table 2. We can see for both data sets, that the use of the HOSP element reduced the error (29) by more than 50%. We remark that in this example there may not be any relation of the mechanical parameters obtained with the solution DMW values.

As we have seen in Example 1, when the parameter α is small numerical problems arise. We have observed the same for the large values, so that in this case the search interval for α was defined as $[0.3, 1.6]$, and the step equal to 0.0025. In Fig. 5 we can see the optimal fitness for both data sets, where the red circles represent the fitness obtained for the data using the porcine liver parameters, and the blue crosses the porcine spleen parameters.

We can appreciate that the use of the HOSP element, provides better accuracy, i.e. a lower value of the fitness function for both DMW data sets. Since in [6] it is concluded that DMW models are appropriate for modeling the behavior of biological tissues, we conclude that the FSLS models are also appropriate, being the HOSP element a better choice than the traditional spring-pot.

Table 2
Results Example 2.

Parameter	Data 1 (spleen)		Data 2 (liver)	
	Spring-pot	HOSP	Spring-pot	HOSP
$\varepsilon_0\,(10^{-6})$	2.18	6.66	9.97	24.48
$E\,(\text{kPa})$	1.24	1.28	3.78	4.22
$\tau'_\varepsilon\,(\text{s}^\alpha)$	90.73	121.53	183.71	229.15
$\tau'_\sigma\,(\text{s}^\alpha)$	57.25	80.58	70.99	101.63
α	1	1.0775	1	1.0865
Fitness (10^{-7})	14.96	2.48	44.78	8.61
Error (10^{-4})	17.061	7.62	29.91	14.64

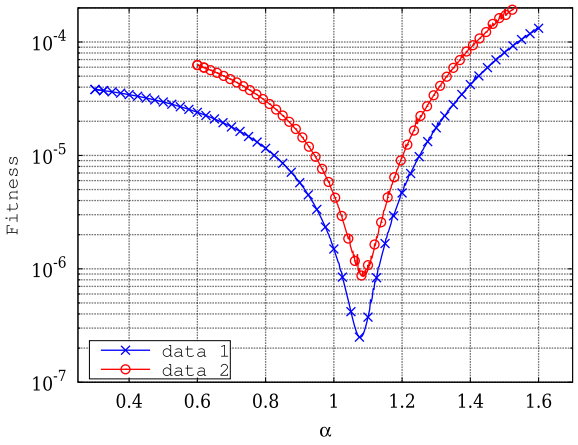

Fig. 5. Example 2 optimal fitness results. (For interpretation of the references to colour in this figure caption, the reader is referred to the web version of this article.)

4.3. Example 3 – Artificial dynamic SLS data

In this example we investigate the effect o the usual quasi-static approximation in the value of the fractional parameter α. In particular, we would like to determine whether an observed high value of α should always be due to a complex constitutive behavior, that we aim to approximate by using a FSLS with a HOSP, or might be artificially caused by the quasi-static approximation. To this aim, we first generate artificial data consistent with the dynamic governing equations and then characterize with the proposed FSLS model which ignores inertial terms. The governing equations correspond to a thin-walled vessel composed of a SLS material and submitted to a variable internal pressure p.

The solution strain is generated using the same procedure of the Example 2. The amplitudes and frequencies are those of the Example 2 multiplied by a factor 10^3 to have magnitudes of the order of the experimental data used in the next example. The stress data is generated from these deformations using the SLS model with parameters $E = 580$ kPa, $\tau_\varepsilon = 0.06$ s, $\tau_\sigma = 0.01$ s, and $\varepsilon_0 = 0$. Then, the pressure and diameter data are obtained by using Eqs. (A.4) and (A.5) of Appendix A. In this way, we generate pressure and diameter values, which are the two measurements that are usually obtained in *in vivo* or *in vitro* experimental procedures. In this example we consider a mass density $\rho = \beta \times 1000$ kg/m^3 with β equal to 1, 5000 and 10,000, to generate three different data sets. For the vessel geometry we consider a reference radius $r_0 = 9.3$ mm, and thickness $h = 0.1\, r_0$.

For the characterization process, the pressure-diameter data is converted to stress–strain data neglecting the inertial terms of the governing equations, i.e. by using the simplified expressions

$$\sigma_\theta = \frac{p\, r}{h}, \quad \varepsilon_\theta = \frac{r - r_0}{r_0}, \tag{32}$$

obtained from (A.4), and (A.5). The optimal fitness functions obtained for the three different values of β are shown in Fig. 6. The parameters obtained for the characterization using each data set are presented in Table 3.

As it is done in Example 1, we compare the results obtained by using the traditional spring-pot and the HOSP element. Fig. 7 shows the hysteresis loops obtained for $\alpha = 1$ (solution for the spring-pot), and the hysteresis for $\alpha = 1.315$ (solution for the HOSP) in the case $\beta = 10,000$.

We remark that a high-order value for α were obtained only for values of density several orders of magnitude higher than the reference value. We conclude that the inertial terms can be neglected when the mechanical parameters are in the order of magnitude of this example. In particular we can assure that the quasi-static approximation cannot be the reason explaining the high-order values for α obtained in actual characterization of arterial mechanical parameters.

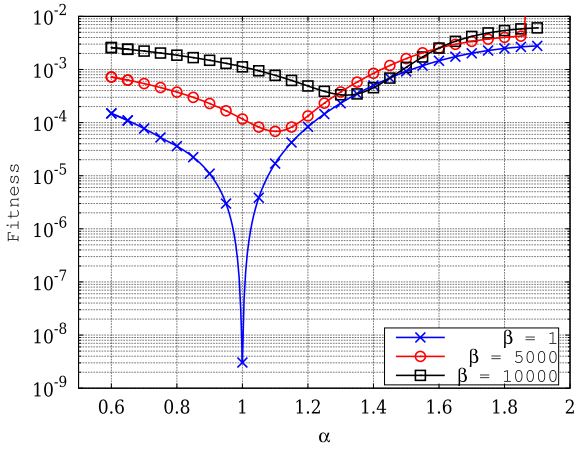

Fig. 6. Example 3 Fitness.

Table 3
Results of Example 3.

Parameter	Solution	$\beta = 1$	$\beta = 5000$	$\beta = 10,000$
$\varepsilon_0\,(10^{-4})$	0	0.0371	46.98	161.17
E(kPa)	580	579.97	597.01	646.11
$\tau'_\varepsilon\,(s^\alpha)$	0.06	0.0599	0.0372	0.0224
$\tau'_\sigma\,(s^\alpha)$	0.01	0.00996	0	0
α	1	1	1.1	1.315
Fitness (10^{-9})		3.042	68,459	329,440
Error (10^{-4})		4.814	113.11	248.07

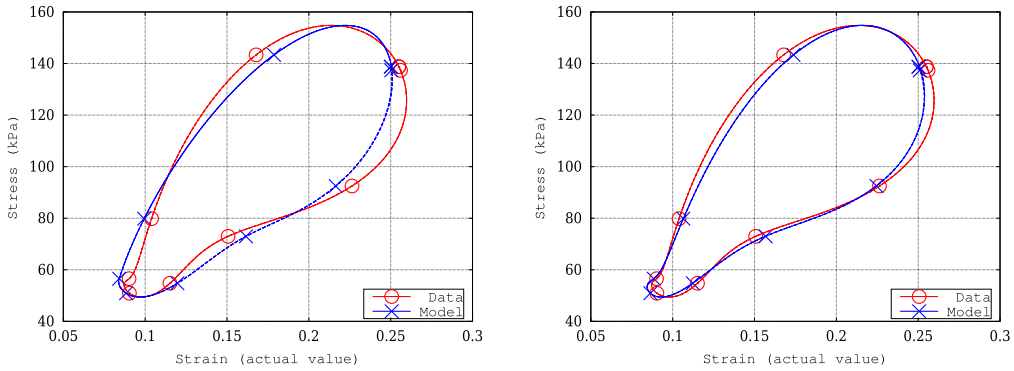

Fig. 7. Example 3: Solutions for $\beta = 10,000$. Left – hysteresis obtained using the spring-pot. Right – hysteresis obtained using the HOSP.

Other complex physical phenomena that are not taken into account in the characterization model, such as fluid–structure interaction, could also affect the value of α. These effects should be investigated in future works.

4.4. Example 4 – Experimental data

In this example the characterization method is applied to arterial wall experimental data. The aim of this example is to show the ability of the proposed FSLS model (with the HOSP element) to fit the data with higher accuracy than the traditional spring-pot and obtain conclusions about the constitutive behavior of the arterial wall.

The experimental data used in this example is part of the data obtained in [9], and consists of measurements of pressure and diameter of a healthy Ascending Aorta of a Merino sheep. The data was acquired with a sampling frequency of 200 Hz. The density measured for the arterial wall is $\rho = 1.06\ \mathrm{g/cm^3}$.

As well as in Example 3, we first generate circumferential stress and strain data assuming a plane strain state, and neglecting the radial component of the stress tensor [2,30]. The expressions of Eq. (32) are used with the thickness-radius ratio approximated by $h/r \approx 0.1$ and with a reference radius $r_0 = 9.36$ mm, which is the mean radius measured in conditions of zero internal pressure, see [9].

Table 4
Results Example 4.

Parameter	Spring-pot	HOSP
$\varepsilon_0\,(10^{-2})$	−2.32	2.98
$E\,(\mathrm{kPa})$	773.3	1037.9
$\tau'_\varepsilon\,(\mathrm{s}^\alpha)$	0.033	0.0076
$\tau'_\sigma\,(\mathrm{s}^\alpha)$	0.0070	0.0028
α	1	1.644
Fitness (10^{-4})	9.33	1.06
Error (10^{-2})	4.545	2.31

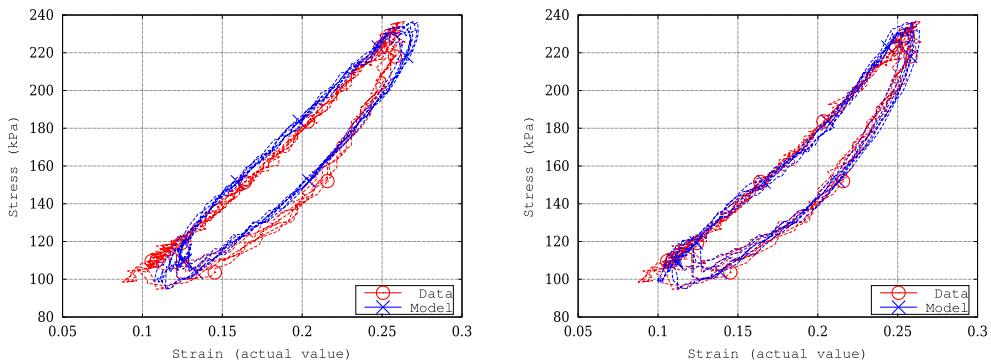

Fig. 8. Example 4: Left – hysteresis obtained using the spring-pot. Right – hysteresis obtained using the HOSP.

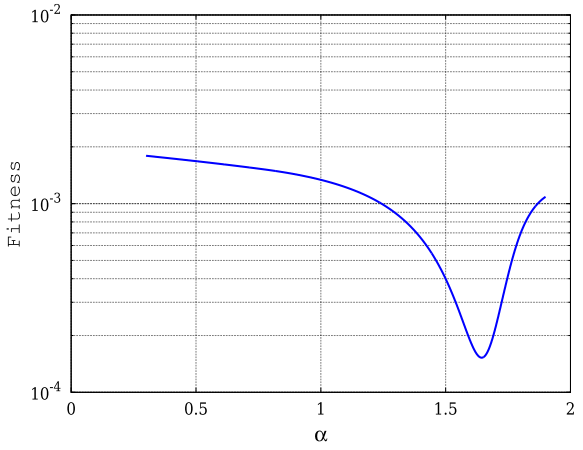

Fig. 9. Example 4 – Fitness results using the HOSP.

The characterization is done using the spring-pot and the HOSP. The results are presented in Table 4. We can see that, as in previous examples, the use of the HOSP element reduces in more than 50% the error and one order of magnitude in the fitness function. Note that the values obtained for the stress-free strain are negligible, therefore we can say that the stress-free radius $\tilde{r} = (1 + \varepsilon_0)r_0$ obtained by the characterization method and the measured value r_0 coincide up to a small error (the stress-free radius $\tilde{r}$ should be understood here as the radius of a static configuration of zero internal pressure, since it is known that residual stresses are present in the arteries [11] and should be considered in thick-walled models).

Fig. 8-left shows the hysteresis loop obtained with the spring-pot, compared with that of the experimental data, and Fig. 8-right shows the same comparison for the HOSP. The improvement in the FSLS model obtained by using the HOSP is clearly noticeable in these figures.

The characterization was performed for all values of α in the interval $[0.3, 1.9]$ whit a step $\Delta\alpha = 0.001$, and the fitness graph obtained is presented in Fig. 9.

5. Discussion

In this paper a numerical method for characterization of mechanical parameters of fractional viscoelastic models was described and validated. The validation was performed through the resolution of three examples with known solution. The method was successfully applied to the modeling of experimental data of arterial wall mechanics.

As it was noted, the results obtained for the Example 1 let us conclude that the method is adequate for characterization of material parameters of a FSLS model, in particular, the fractional parameter was obtained accurately even when noisy data was used.

The results of Example 2 show that the use of a HOSP element enhances the ability of a FSLS constitutive model to represent a complex behavior corresponding to a DMW model. The mechanical parameters used for the data generation correspond to porcine spleen and porcine liver, therefore we conclude that the proposed model can be used for properly modeling the behavior of these biological tissues. Future works should investigate the ability of the FSLS model with a HOSP to represent accurately the behavior of other tissues that are usually modeled with the DMW and Triple Maxwell-arm Wiechert models.

In Example 3, the characterization was performed using data obtained by solving the dynamic governing equations of a thin-walled vessel under internal pressure. The mechanical parameters and density used are in the order of those obtained in Example 4 for the arterial wall tissue. It was shown that for reasonable values of the mass density the inertial terms can be neglected, i.e. the quasi-static approximation does not introduce a noticeable error in the value of the fractional parameter α obtained by the characterization method. The quasi-static approximation can be used in characterization using experimental data as it was done in Example 4.

In Example 4 we obtained an important result about the use of the HOSP in FVMs for arterial wall modeling instead of the traditional spring-pot. The results show clearly that the HOSP improves the fit of the experimental data. In the literature, histological interpretations have been given to the fractional parameter value bounded by one. Further studies should investigate possible histological interpretations of a fractional parameter greater than one. However, even if no interpretation is provided yet, a better modeling is obtained, which could lead to improvements in cardiovascular simulations.

Acknowledgments

The authors would like to thank the financial support of the Uruguayan National Research and Innovation Agency (ANII project code FMV-3–2011-1-6125) and the "Comisión Sectorial de Investigación Científica (CSIC)".

Appendix A. Dynamic Standard Linear Solid equations

In this section we present the governing equations of a Standard Linear Solid material considering dynamic contribution. This model is given by a SLS constitutive model, and the contribution of the acceleration in the equations of motion. Given a solid with density ρ, the mechanical balance equations are given by

$$\nabla \cdot T + b = \rho \ddot{u}, \tag{A.1}$$

where b is the load density, T is the Cauchy stress tensor, and u the displacement vector.

Let us consider now a thin-walled vessel with internal pressure p at a plane strain deformation state with negligible axial and radial stresses. The internal pressure divided by the wall thickness is considered as a volume load, so that the balance equation is non-trivial only in the radial component. The following expression for the stress σ_θ is then obtained:

$$\frac{-\sigma_\theta}{r} + \frac{p}{h} = \rho \ddot{u}_r. \tag{A.2}$$

Since $\varepsilon_\theta = u_r/r_0$, where r_0 is the reference radius, we obtain

$$\sigma_\theta = \frac{pr}{h} - \rho\, r_0\, r\, \ddot{\varepsilon}_\theta. \tag{A.3}$$

We are now able to obtain an expression for the internal pressure in terms of the stress, the strain, the density and the thickness-radius ratio as:

$$p = h\frac{\sigma_\theta}{r} + \rho\, h\, r_0\, \ddot{\varepsilon}_\theta. \tag{A.4}$$

The radius can be obtained by using $r = r_0 + u_r$ and $\varepsilon_\theta = u_r/r_0$ as:

$$r = r_0(1 + \varepsilon_\theta). \tag{A.5}$$

Appendix B. High-order spring-pot element justification

In this section we show that it is physically admissible to consider a HOSP element as was described. Let us consider a spring-pot element with a fractional response of order α, we will show that the constraint $\alpha \leqslant 2$ can be used instead of $\alpha \leqslant 1$, without violating thermodynamic constraints. This result allows the use of this element in constitutive models. We will obtain a relation for the parameters in a similar way as it is done in the literature [17,18].

Let us consider that the strain and stress functions can be decomposed in Fourier series,

$$\varepsilon(t) = \sum_{i=0}^{\infty} \varepsilon_i e^{j\lambda_i t} \quad \sigma(t) = \sum_{i=0}^{\infty} \sigma_i e^{j\lambda_i t}. \tag{B.1}$$

where j is the imaginary unit $j^2 = -1$. The complex coefficients ε_i and σ_i must be such that ε and σ be real valued function. Since the constitutive equation of the HOSP is satisfied, we obtain:

$$\sigma(t) = E_1\, \tau'^{\alpha}_{\sigma} D^{\alpha} \varepsilon(t) \quad \Rightarrow \quad \sigma_i = E_1\, \tau'^{\alpha}_{\sigma} (j\lambda_i)^{\alpha} \varepsilon_i. \tag{B.2}$$

In the same manner we obtain the coefficients of the series of the first derivative of the strain:

$$\dot{\varepsilon}(t) = \sum_{i=0}^{\infty} j\,\lambda_i \varepsilon_i e^{j\lambda_i t} \quad \Rightarrow \quad \dot{\varepsilon}_i = j\,\lambda_i \varepsilon_i. \tag{B.3}$$

In order to validate a constitutive model, we have to check that the thermodynamic laws are satisfied. In particular we will analyze closed processes, where the dissipation must be nonnegative [31,32]. Let us consider a thermodynamic closed process where thermal influences are negligible and the solid conductivity is high enough to produce a zero gradient of temperature. The rate of internal work is equal to the rate of free energy plus the dissipation

$$\dot{w} = \dot{\psi} + \delta. \tag{B.4}$$

Since the free energy ψ is a state variable, the integral of $\dot{\psi}$ in any closed process with period T is zero, thus, we obtain the following equality

$$\int_0^T \dot{w}\, dt = \int_0^T \delta\, dt \geqslant 0. \tag{B.5}$$

The first integral can be calculated by the following expression

$$\int_0^T \dot{w}\, dt = \int_0^T \langle \sigma, \dot{\varepsilon} \rangle\, dt \tag{B.6}$$

and substituting the expressions in Eqs. (B.2) and (B.3) we obtain:

$$\int_0^T \dot{w}\,dt = \int_0^T \left(\sum_{i=0}^{\infty} E_1\,\tau'_\sigma\,(j\lambda_i)^\alpha \varepsilon_i\, e^{j\lambda_i t}\right)\left(\sum_{i=0}^{\infty} j\,\lambda_i \varepsilon_i\, e^{j\lambda_i t}\right) dt. \tag{B.7}$$

The exponential functions form an orthogonal basis, thus, the integral of any product between different frequencies exponentials will be zero. Moreover, since the positive dissipation inequality is required for any process, all the terms in the sum must be positive thus we obtain the following equivalent inequalities:

$$Re\left(E_1\,\tau'_\sigma\,\lambda_i^\alpha j^\alpha\,\varepsilon_i\,(-j\lambda_i\bar{\varepsilon}_i)\right) \geqslant 0 \quad \Longleftrightarrow \quad Im\left(|\varepsilon_i|^2\,E_1\,\tau'_\sigma\,\lambda_i^\alpha j^\alpha\,\lambda_i\right) \geqslant 0, \tag{B.8}$$

substituting the expression for j^α in the second inequality, we obtain a constraint for the parameter α

$$E_1\tau'_\sigma \sin\left(\alpha\frac{\pi}{2}\right) \geqslant 0. \tag{B.9}$$

Since E_1 and τ_σ are positive constants, we conclude that α must belong to the interval $[0,2]$ in order to obtain a thermodynamically consistent high-order element. Repeating the procedure with the FSLS equation we obtain the relation

$$E(\tau'_\varepsilon - \tau'_\sigma)\sin\left(\alpha\frac{\pi}{2}\right) \geqslant 0, \tag{B.10}$$

where, from the definitions of τ'_ε and τ'_σ in Eq. (16), we can see $\tau'_\varepsilon - \tau'_\sigma \geqslant 0$. Finally, we obtain the same feasible interval for the parameter α.

In addition, we notice that the positive internal work rate constraint can be also presented as a simple geometrical condition of the hysteresis graph. Let us consider the plane curve $\mathscr{C} : (\varepsilon(t), \sigma(t))$ where σ and ε are real valued. Since the coordinates functions are periodic the curve define a two-dimensional area Ω with normal vector $n = (0,0,-1)$. Let us consider the vector field $\vec{X} = (\sigma, 0, 0)$ and the expression of its circulation in $\mathscr{C}$

$$\int_{\mathscr{C}} \vec{X}\cdot\vec{t}\,ds = \int_{\mathscr{C}} \sigma\,\dot{\varepsilon}\,dt. \tag{B.11}$$

This circulation can also be calculated applying the Stokes theorem

$$\int_{\mathscr{C}} \vec{X}\cdot\vec{t}\,ds = \int_\Omega \left(0,0,-\frac{\partial\sigma}{\partial\sigma}\right)\cdot(0,0,-1)\,dA = \int_\Omega 1\,dA. \tag{B.12}$$

Then we obtain the following equality:

$$\int_0^T \sigma\,\dot{\varepsilon}\,dt = \text{Area}(\Omega). \tag{B.13}$$

Since the internal work rate is positive, the area must be positive. In this way the thermodynamic condition is converted into a clockwise orientation of the curve $\mathscr{C}$ in the space (ε, σ) condition.

In order to verify numerically the results we generate graphs similar to those shown in [21] for values of α higher than one. The constitutive model used for this data is the Fractional Kelvin–Voigt model, defined by a spring and a spring-pot in parallel. The mechanical parameters used are $E = 1000$ kPa, $\tau_\varepsilon = 0.1$ s$^\alpha$ and, frequency $\lambda = 10$ rad/s. Since the model is

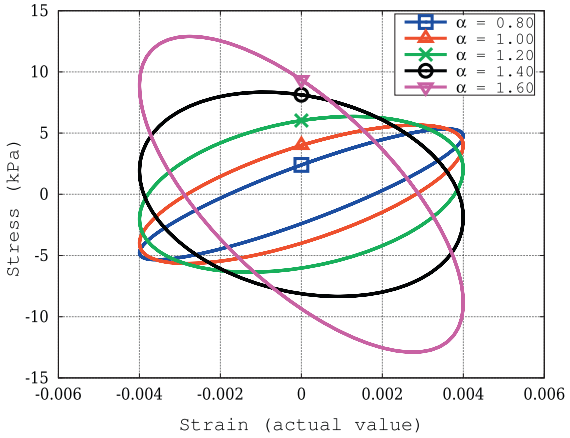

Fig. B.10. Fractional Kelvin–Voigt hysteresis.

Kelvin–Voigt, we consider $\tau_\sigma = 0$. Fig. B.10 shows the ellipses for various values of α. When α tends to the value 0 the ellipse collapses into a line with slope $E(1+\tau_\varepsilon)$, while for $\alpha \to 2$ the ellipse collapses into a line with slope $E(1-\lambda^2\tau_\varepsilon)$.

It is important to remark that within the interval $[0,2]$ all the curves are clockwise oriented. For α higher than 2 the curve $\mathscr{C}$ becomes counterclockwise oriented, thus the ellipse area becomes negative, which is not thermodynamically admissible.

The mathematical results presented demonstrate the high-order spring-pot element can be used to model real materials.

References

[1] L. Fan, L. Wong, G. Ma, Experimental investigation and modeling of viscoelastic behavior of concrete, Constr. Build. Mater. 48 (2013) 814–821.
[2] Y.C. Fung, Biomechanics, Mechanical Properties of Living Tissues, Springer, New York, NY, 1981, http://dx.doi.org/10.1007/978-1-4757-1752-5. <http://link.springer.com/10.1007/978-1-4757-1752-5>.
[3] Y.C. Fung, Biomechanics, second ed., Circulation, Springer, 1997.
[4] C. Then, T.J. Vogl, G. Silber, Method for characterizing viscoelasticity of human gluteal tissue, J. Biomech. 45 (2012) 1252–1258.
[5] M. Zhang, P. Nigwekar, B. Castaneda, K. Hoyt, J.V. Joseph, A. di Sant'Agnese, E.M. Messing, J.G. Strang, D.J. Rubens, K.J. Parker, Quantitative characterization of viscoelastic properties of human prostate correlated with histology, Ultrasound Med. Biol. 34 (2008) 1033–1042.
[6] X. Wang, J.A. Schoen, M.E. Rentschler, A quantitative comparison of soft tissue compressive viscoelastic model accuracy, J. Mech. Behavior Biomed. Mater. 20 (2013) 126–136.
[7] M. Naghavi, P. Libby, E. Falk, S.W. Casscells, S. Litovsky, J. Rumberger, J.J. Badimon, C. Stefanadis, P. Moreno, G. Pasterkamp, Z. Fayad, P.H. Stone, S. Waxman, P. Raggi, M. Madjid, A. Zarrabi, A. Burke, C. Yuan, P.J. Fitzgerald, D.S. Siscovick, C.L. de Korte, M. Aikawa, K.E. Juhani Airaksinen, G. Assmann, C.R. Becker, J.H. Chesebro, A. Farb, Z.S. Galis, C. Jackson, I.-K. Jang, W. Koenig, R. a. Lodder, K. March, J. Demirovic, M. Navab, S.G. Priori, M.D. Rekhter, R. Bahr, S.M. Grundy, R. Mehran, A. Colombo, E. Boerwinkle, C. Ballantyne, W. Insull, R.S. Schwartz, R. Vogel, P.W. Serruys, G.K. Hansson, D.P. Faxon, S. Kaul, H. Drexler, P. Greenland, J.E. Muller, R. Virmani, P.M. Ridker, D.P. Zipes, P.K. Shah, J.T. Willerson, From vulnerable plaque to vulnerable patient: a call for new definitions and risk assessment strategies: Part I, Circulation 108, 2003, 1664–1672.
[8] D. Bessems, C.G. Giannopapa, M.C.M. Rutten, F.N. van de Vosse, Experimental validation of a time-domain-based wave propagation model of blood flow in viscoelastic vessels, J. Biomech. 41 (2008) 284–291.
[9] D. Valdez-Jasso, M.A. Haider, H.T. Banks, D. Bia Santana, Y. Zócalo Germán, R.L. Armentano, M.S. Olufsen, Analysis of viscoelastic wall properties in ovine arteries, IEEE Trans. Bio-med. Eng. 56 (2009) 210–219.
[10] R. Lakes, Viscoelastic Materials, first ed., Cambridge University Press, 2009.
[11] G.A. Holzapfel, T.C. Gasser, R.W. Ogden, A new constitutive framework for arterial wall mechanics and a comparative study of material models, J. Elasticity 61 (2000) 1–48.
[12] D. Valdez-Jasso, D. Bia, Y. Zócalo, R.L. Armentano, M. a. Haider, M.S. Olufsen, Linear and nonlinear viscoelastic modeling of aorta and carotid pressure-area dynamics under in vivo and ex vivo conditions, Ann. Biomed. Eng. 39 (2011) 1438–1456.
[13] G.W. Scott Blair, The role of psychophysics in rheology, J. Colloid Sci. 2 (1947) 21–32.
[14] M. Stiassnie, On the application of fractional calculus for the formulation of viscoelastic models, Appl. Math. Modell. 3 (1979) 300–302.
[15] I. Podlubny, Fractional Differential Equations, first ed., Academic Press, 1999.
[16] R.L. Bagley, P.J. Torvik, A theoretical basis for the application of fractional calculus to viscoelasticity, J. Rheol. 27 (1983) 201–210.
[17] R.L. Bagley, P.J. Torvik, On the fractional calculus model of viscoelastic behavior, J. Rheol. 30 (1986) 133–155.
[18] C. Friedrich, Relaxation functions of rheological constitutive equations with fractional derivatives: Thermodynamical constraints, in: J. Casas-Vázquez, D. Jou (Eds.), Rheological Modelling: Thermodynamical and Statistical Approaches, Springer, Berlin, Heidelberg, 1991, pp. 321–330. <http://link.springer.com/chapter/10.1007/3-540-53996-448>.
[19] M. Allam, A.M. Zenkour, Bending response of a fiber-reinforced viscoelastic arched bridge model, Appl. Math. Modell. 27 (2003) 233–248.
[20] S.W. Welch, R.A. Rorrer, R. Duren Jr., Application of time-based fractional calculus methods to viscoelastic creep and stress relaxation of materials, Mech. Time-Depend. Mater. 3 (1999) 279–303.
[21] R. Lewandowski, B. Choryczewski, Identification of the parameters of the KelvinVoigt and the Maxwell fractional models, used to modeling of viscoelastic dampers, Comput. Struct. 88 (2010) 1–17.
[22] V. Djordjević, J. Jarić, B. Fabry, J.J. Fredberg, D. Stamenović, Fractional derivatives embody essential features of cell rheological behavior, Ann. Biomed. Eng. 31 (2003) 692–699.
[23] D. Craiem, R.L. Armentano, A fractional derivative model to describe arterial viscoelasticity, Biorheology 44 (2007) 251–263.
[24] D. Craiem, F.J. Rojo, J.M. Atienza, R.L. Armentano, G.V. Guinea, Fractional-order viscoelasticity applied to describe uniaxial stress relaxation of human arteries, Phys. Med. Biol. 53 (2008) 4543–4554.
[25] D.O. Craiem, F.J. Rojo, J.M. Atienza, G.V. Guinea, R.L. Armentano, Fractional calculus applied to model arterial viscoelasticity, Latin Am. Appl. Res. 38 (2008) 141–145.
[26] J.G. Liu, M.Y. Xu, Higher-order fractional constitutive equations of viscoelastic materials involving three different parameters and their relaxation and creep functions, Mech. Time-Depend. Mater. 10 (2006) 263–279.
[27] J.M. Pérez Zerpa, A. Canelas, B. Sensale, D. Bia Santana, R.L. Armentano, A high-order viscoelastic fractional element applied to modeling ovine arterial wall behavior, in: Proceedings of the 11th World Congress on Computational Mechanics (WCCM XI), Barcelona, 2014.
[28] J.W. Eaton, D. Bateman, S. Hauberg, R. Wehbring, GNU Octave version 3.8.1 manual: a high-level interactive language for numerical computations, CreateSpace Independent Publishing Platform, 2014. <http://www.gnu.org/software/octave/doc/interpreter>.
[29] S.P.C. Marques, G.J. Creus, Computational Viscoelasticity, Springer, Heidelberg, 2012.
[30] R.L. Armentano, J. Barra, J. Levenson, Arterial wall mechanics in conscious dogs assessment of viscous, inertial, and elastic moduli to characterize aortic wall behavior, Circ. Res. 76 (1995) 468–478.
[31] M. Silhavý, The Mechanics and Thermodynamics of Continuous Media, Springer-Verlag, Berlin, Heidelberg, New York, 1997.
[32] M.E. Gurtin, E. Fried, L. Anand, The Mechanics and Thermodynamics of Continua, Cambridge University Press, 2009.